Northumbria University NEWCASTLE

KD6040

Individual Physics Project

Final Report

MPhys (Hons) Physics with Astrophysics

2022/2023

Diamagnetic Accretion Disc Dynamics in Non-Equatorial Elliptical Orbits around Spinning Magnetic White Dwarfs

Name of Student: Penelope du Bois
Name of Supervisor: Graham Wynn

May 4th, 2023

Declaration

I hereby declare that the work contained in this document is all my own work. I also confirm that when this work uses ideas and opinions from the work of others, these are credited in full by citing the corresponding references.
Name: Penelope du Bois
Signature: *Penelope du Bois*
Date: May 4th, 2023

Contents

Abstract

Current observations of accretion discs around magnetic white dwarfs indicate that they exhibit inconsistent accretion rates, which deviate from the predictions of models based on Poynting-Robertson drag and diamagnetic drag. In general, simulated white dwarfs harbour discs with longer accretion lifespans than can be supported by current data, implying that in reality the drag force on orbiting particles is higher than can currently be explained or simulated. This discrepancy between observed and simulated accretion lifetimes is known as the missing disc problem. In this paper, we propose a new approach to address this issue by exploring the impact of white dwarf angular momentum on accretion rates, also investigating how orbits at differing angles to the white dwarf's magnetic moment affect the dynamics of these discs. Through these simulations we found that the spin of a white dwarf can significantly affect the accretion timescale of an orbiting disc, decreasing it by up to an order of magnitude in extreme conditions. We also found that particles in orbits passing over the poles of a white dwarf experienced more magnetic drag than orbits around the equator and so were accreted faster than those in a more equatorial orbit. Moreover, we observed a new phenomenon where particles are accelerated by the magnetic field and ejected from the white dwarf's gravitational well under certain configurations of spin and orbital plane. Our results suggest that white dwarf angular momentum and differing orbital geometries have a measurable affect on accretion timescales, which could partially account for the missing disc problem.

List of Figures

List of Tables

1 Introduction

1.1 Overview

White dwarfs (WDs) are a class of extremely dense stellar objects, on average having masses comparable to the sun with radii roughly the same as the earth. As many as 25% of the stars within 10pc of the sun may be WDs (Carroll and Ostlie 2017) and they are thought to be the final state for approximately 97% of stars in the Milky Way Galaxy (Fontaine, Brassard, and Bergeron 2001).

WDs form when stars with less than 8 solar masses fail to undergo supernova, instead becoming red giants and eventually shedding their outer layers and forming planetary nebula. Due to this, WDs are essentially the C-O (carbon-oxygen) core of old red giants. At this point WDs no longer have the required pressure to continue fusing elements and so start to cool from temperatures exceeding $10^6 K$ right after forming. This cooling is predicted to continue until the star reaches temperatures of around $1000K$ and becomes a black dwarf, although this is expected to take longer than the current estimated lifetime of the observable universe (Carroll and Ostlie 2017).

WDs are only able to resist collapse against their high gravity due to electron degeneracy pressure, a quantum mechanical phenomenon which relies on the Pauli exclusion principle, stating that no two electrons (and all other fermions) can occupy the same quantum state around an atom. This produces additional pressure in extremely dense materials resisting gravitational collapse in WDs. This degeneracy pressure can be used to calculate the Chandrasekhar limit, the highest mass a WD can approach before collapsing into a neutron star, for a non-rotating WD this mass is approximately 1.44 solar masses (Chandrasekhar 1931).

WDs can be classified into several groups depending on observed absorption lines in their spectra, dictating the presence of specific elements in their atmospheres. Roughly two thirds of WDs are classified under DA, displaying only evidence of hydrogen absorption, type DB show helium absorption lines and type DC show no absorption lines at all, these two classes make up 8% and 14% respectively (Carroll and Ostlie 2017). The classes DZ and DAZ are observed to have evidence of metals in their spectra, and make up around 15-35% of catalogued WDs (Zuckerman et al. 2003; Xu and Jura 2012) (for our purposes, 'metallic' is used here to refer to any elements heavier than hydrogen and helium).

The primary explanation for the presence of this metal pollution in WD atmospheres is thought to be through the capture and accretion of asteroids into debris discs (Jura 2003). This occurs when an asteroid passes too close to a WD and is broken up into a stream of small particles by tidal forces, which then accrete onto the WD, losing angular momentum due to various forces (Rafikov 2011). We believe that in some scenarios these discs may be ejected from WD systems by being accelerated by the WD, reaching escape velocity after some time.

Accretion is an astrophysical process in which material in an orbit around a gravitational well loses angular momentum, accumulating into a more massive object over time. This occurs through different forms of interaction with other objects in in gravitational well, such as collisions, heating, and various drag forces. A large portion of accreting objects around massive bodies are thought to take the form of accretion discs, large structures consisting of a ring of material which occupies one orbit, usually around a star. In this paper we refer to the time taken for a particle to fully accrete onto a larger body as the accretion timescale for that particle.

The ejection of an object from a gravitational well is a process which can be likened to the accretion mechanism but in reverse, where the object will instead gain angular momentum over time from other nearby objects. In order to eject an object and accelerate it to the escape velocity of a system, the total angular momentum and energy of all objects in the gravitational well will by reduced. The required velocity to escape a gravitational well is derived from Newton's laws of gravitation and is given by:

$$v_e = \sqrt{\frac{2GM}{d}} \tag{1}$$

Where v_e is the escape velocity, G is the universal gravitational constant, M is the mass of the source of the gravity well, and d is the distance from the centre of the well. We refer to the time taken for a particle to escape one of these systems as the ejection timescale for that particle.

As these discs are formed from asteroids which break up due to tidal forces, we expect them to form starting at the periapsis of a very eccentric orbit where the forces will be maximised. We also expect these orbits to be highly eccentric ($e > 0.99$) where the periapsis is significantly closer to the WD than the apoapsis. We can calculate the ratio from the formula (Robbin 1981):

$$e = \frac{r_a - r_p}{r_a + r_p} \tag{2}$$

Where e is the orbital eccentricity, r_a is the apoapsis (the highest point of the orbit), and r_p is the periapsis (the lowest point of the orbit). From this we find the ratio of r_a to r_b for an eccentricity of $e = 0.99$ to be ~ 200, and so see that the apoapsis of an average accretions disc would be over 200 times further away from the WD than the periapsis.

1.2 Poynting-Robertson Drag

In non magnetic WDs Poynting-Robertson (PR) drag is considered to be the main driver of accretion with the force felt on a particle being proportional to incident radiation from the star (Burns, Lamy, and Soter 1979). PR drag is caused as incident radiation on a particle opposes its motion, leading to a drop in angular momentum and it spiraling into the star. Due to the particle's motion around a star, from the star's frame of reference, this incident radiation appears to interact with the particle from a forward direction creating a small force in the opposite direction.

As in reality these discs are physical object with 3 dimensional depth, this incident radiation is blocked from reaching all particles in the accretion disc by other particles closer to the inner rim of the disc. Shielded particles in these optically thick discs are affected by PR drag to a significantly lower force due to PR drag and so have far lower accretion rates.

When PR drag is applied to unshielded particles in optically thin discs, simulated accretion timescales are found to be 10-100 years, however real world observations imply that

discs take far longer to fully accrete (Farihi 2016). Accounting for optically thick discs, accretion timescales are greatly lengthened (Rafikov 2011) and estimations of the accretion of debris discs in WD systems where shielded PR drag is the dominant force show lifetimes in the order of Myrs (Farihi, Jura, and Zuckerman 2009). This implies that the majority of the population of polluted WDs should have debris discs while current observations, however, show only around 0.8-6.5% of polluted WDs harbour observable debris discs (Debes, Sigurdsson, and Hansen 2007; Farihi 2016). This deviation between expected accretion timescales and observed timescales is known as the missing disc problem.

1.3 Magnetic Drag

In the case of magnetic WDs accretion is thought to be primarily caused by magnetic drag forces (Hogg, Cutter, and Wynn 2021) as the majority of material observed in polluted WD atmospheres is metallic (Koester, Gänsicke, and Farihi 2014) and observed magnetic WDs have higher accretion rates (Kawka and Vennes 2014). These forces can present in various different ways such as in eddy currents or magnetorotational instability, which cause drag and turbulence in an accretion disc respectively (Balbus and Hawley 1991).

The magnetic force we choose to investigate in this paper is diamagnetism, a phenomenon which is most easily visible via the quantum mechanical Meissner effect in superconductors (Bardeen, Cooper, and Schrieffer 1957) where field lines are warped around a superconducting object. Any diamagnetic object moving relative to a magnetic field experiences a drag force opposing its motion, this is caused by the generation of an induced current in the object described by Faraday's Laws. According to Lenz's Laws this current then produces its own magnetic field around the object which opposes the original magnetic field, causing a drag force also known as magnetic breaking (Berry and Geim 1997; Kuestler 2007). The relative velocity between the object and the external magnetic field determines both the magnitude and direction of the drag force produced (Drell, Foley, and Ruderman 1965).

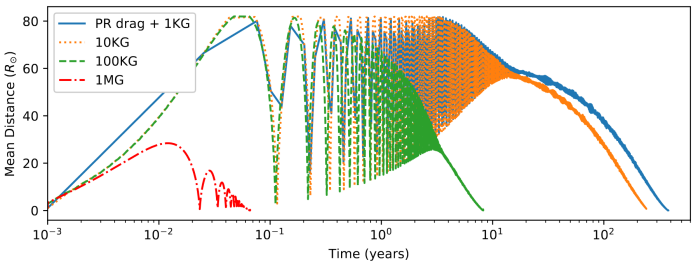

Figure 1: Mean particle distance against time for various magnetic field strengths (Hogg, Cutter, and Wynn 2021).

Simulations which incorporate diamagnetic drag (Hogg, Cutter, and Wynn 2021) are able to demonstrate that magnetic breaking reduces disc lifetimes for WDs with magnetic field strengths above $\sim 10kG$ for optically thick discs, while strengths above $\sim 100kG$ are required to noticeably shorten lifetimes for optically thin discs. They also show that with field strengths above 1MG, accretion onto the WD occurs in less than one year, this can be seen in Table 1. Additionally they show that, except for in circumstances with high magnetic fields, orbital discs are circularised before being accreted due to the most force being applied to particles at their periapsis.

They note that accretion rates are highly dependant on magnetic field strength, disc pericentre distance, and particle size, meaning accretion timescales produced in simulations will likely not cover all real world scenarios. Also noting that accounting for diamagnetism alone cannot entirely explain the missing disc problem, but does partially explain some observations of DB and DA WDs with no discs. They finally suggest that there is a possibility that a large proportion of polluted WDs may harbour a magnetic field below the range of detectable values.

2 Aims and Objectives

The main aim of this paper is to expand on the work done by Hogg, Cutter, and Wynn (2021), in simulating the motion of dust particles in orbit of magnetic WDs. We will improve on their WD simulation by modeling WDs with angular velocity and simulate accretion discs with orbital planes at different angles to the WD equator. This will be done in order to demonstrate how accretion timescales are effected by both a rotating magnetic field, and orbits which pass through the magnetic field at varying angles. There are 3 main objectives which will need to be completed in order to obtain this aim.

2.1 Literature Review

Initially a literature report will be completed in order to collect up to date information about WDs and their accretion discs. This will focus on collecting data which will be useful in producing a computational model such as specific values pertaining to important WD characteristics as well as parameters concerning particles in their orbit. We will also investigate the equations which describe the forces which operate on these orbiting dust particles. This literature review will be necessary in ensuring that our final model will accurately reflect reality and produce useful results.

2.2 Simulation Development

These parameters and equations of force will then be used to produce a piece of code which can simulate an amount of particles in a gravitational potential around a magnetic WD. Once we are confident in the accuracy of this initial model we will begin to add additional forces which should reflect how these particles would behave in orbit around a real magnetic WD. The results of this simulation will be checked against those previous papers to allow us to further tune the model to produce accurate results, giving us a basis on which to add additional complexity and collect novel data.

2.3 Simulation Results

The code will then be adapted to simulate WD's with varying angular velocity, magnetic moment direction, and different starting conditions for particles in accretion discs. This simulation will then be run, first by varying the rotation of the white dwarf to determine the effect angular momentum has on accretion. Then the geometry of the system will be

investigated by measuring accretion with a various axes of angular momentum and debris disc orbit. This will give us a wide range of results in various conditions which have not yet been investigated in other papers.

2.4 Overall Aim

This project aims to produce a model of magnetic WD accretion mechanics which considers more factors than previously studied in an attempt to produce results which allow us to investigate new conditions. We believe this data may work to explain the WD missing disc problem if higher accretion rates are observed under these new conditions. Additionally, as we predict this model will give us data for particles which are ejected from the system, we will be able to investigate data for ejection timescales.

3 Methodology

3.1 Mathematical Background

3.1.1 Force due to Gravity

We choose to use Newton's equations of universal gravitation will to describe the motion of particles in a potential well. We do not expect particles in these systems to move fast enough or move through strong enough gravitational wells to encounter relativistic phenomena and so Newton's laws will be used instead of general relativity. We can calculate a maximum expected velocity for the particle using the equation (Bate, Mueller, and White 1971):

$$v \approx \sqrt{\frac{GM_{WD}}{r}} \tag{3}$$

Where v is an estimate for particle speed, G is the universal gravitational constant, M_{WD} is the WD mass, and r is the particle's distance from the WD. We see that in orbit, at the WD surface, a particle would be travelling with velocity $v \approx 3 \times 10^6$, 1% the speed of light $c \approx 3 \times 10^8$. We then calculate the Lorentz factor for an object moving this speed using the equation:

$$\gamma = \frac{1}{\sqrt{1 - \frac{v^2}{c^2}}} \tag{4}$$

Where v is the objects velocity and c is the speed of light. We find a worst case gamma factor of $\gamma \approx 1.00005$, and so are confident relativistic effects will have very little affect on our results over our expected timescales.

The equation for the force felt on a particle from gravity is then given by (Newton 1726):

$$F_g = -G\frac{M_{WD}m_p}{r^2} \tag{5}$$

Where G is the universal gravitational constant, M_{WD} is the WD mass, m_p is the particle mass, and r is the distance from the centre of the WD.

3.1.2 Force due to Poynting-Robertson Drag

The force due to PR drag can be derived by understanding it as a result of the radiation pressure felt on a particle from the WD's incident starlight. This means the force is proportional to the area of the particle ($F_{PR} \propto r_p^2$) and so, as gravitational force varies with mass ($F_G \propto r_p^3$), smaller particles are affected significantly more than larger ones. Using this we can derive a formula to calculate the force felt on a particle from PR drag and parameterise the force using the following equation (Guess 1962):

$$F_{PR} = -\frac{v}{c^2}W = -\frac{{r_p}^2 L_{WD}}{4c^2}\sqrt{\frac{GM_{WD}}{r^5}} \tag{6}$$

Where v is the particle's velocity, c is the speed of light, W is the power of incoming radiation, r_p is the particle's radius, M_WD is the WD mass, L_{WD} is the WD luminosity, and r is the particle's orbital radius. We see that as the force varies with $r^{-2.5}$, the drag increases relative to gravity as a particle approaches the WD, this tends to circularise the orbit before particles fully accrete on to the WD (Abd El-Salam 2018).

3.1.3 Force due to Magnetic Field

By assuming the magnetic field around the WD approximately represents a magnetic dipole at large radii we can use the following formula to calculate the magnitude and direction of the field strength at a point r around the WD (Griffiths 2013):

$$B(r) = \frac{\mu_0}{4\pi}\left(\frac{3r(m \cdot r)}{r^5} - \frac{m}{r^3}\right) \tag{7}$$

Where μ_0 is the vacuum permeability constant, r is a point in space around the white dwarf and m is the magnetic moment.

The force felt from diamagnetic drag is proportional to the velocity of a particle with respect to the magnetic field due to it being a force arising from the motion of a body through field lines causing their displacement. From this we parameterise the force on a diamagnetic dust particle due to the magnetic field by (King 1993; Wynn and King 1995; Hogg, Cutter, and Wynn 2021):

$$F = -k(r)m_p v_r \tag{8}$$

Where k is a diamagnetic drag coefficient, m_p is the particle mass, and v_r is the relative velocity between the local magnetic field and the particle.

The drag coefficient $k(r)$ is determined by local magnetic field strength, particle size, composition, and charge, taking the form (Hogg, Cutter, and Wynn 2021):

$$k(r) = k_0\left(\frac{r}{R_\star}\right)^{-6}\sqrt{1 + 3\frac{z_p^2}{r^2}} \tag{9}$$

Where r is the distance from the centre of the white dwarf, $R_\star$ is the white dwarf radius, z_p is the position of the particle along the spin/dipole axis, and k_0 is the diamagnetic drag coefficient at the white dwarf surface, thought to be related to particle lifetime via the equation (Hogg, Cutter, and Wynn 2021):

$$k(r) \approx \frac{1}{T_L} \tag{10}$$

Where T_L is the particle lifetime given by:

$$T_L \approx \rho R_p \frac{8\pi}{B(r)^2}\sqrt{\frac{GM_{WD}}{R_\star}} \tag{11}$$

Where ρ is the particle density, R_p is the particle radius, $B_\star$ is the magnetic field strength at the white dwarf surface, G

is the universal gravitational constant, M_{WD} is the white dwarf mass, and $R_\star$ is the white dwarf radius. This then gives us the value for k_0:

$$k_0 \approx \left(\rho R_p \frac{8\pi}{B_\star^2}\sqrt{\frac{GM_{WD}}{R_\star}}\right)^{-1} \tag{12}$$

Where ρ is the particle density, R_p is the particle radius, $B_\star$ is the magnetic field strength at the white dwarf surface, G is the universal gravitational constant, M_{WD} is the white dwarf mass, and $R_\star$ is the white dwarf radius.

Combining all of these equations we find the force due to diamagnetic drag as:

$$F = -m_p v_r \left(\rho R_p \frac{8\pi}{B_\star^2}\sqrt{\frac{GM_{WD}}{R_\star}}\right)^{-1} \left(\frac{r}{R_\star}\right)^{-6} \sqrt{1+3\frac{z_p^2}{r^2}} \tag{13}$$

3.1.4 Alfvén Radius

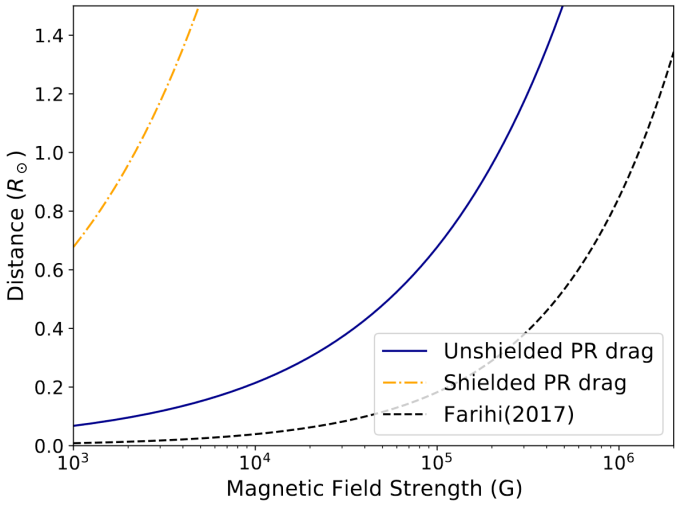

Figure 2: Alfvén radius for the cases of shielded and unshielded PR drag (Hogg, Cutter, and Wynn 2021) compared to previously calculated radii (Farihi, Hippel, and Pringle 2017).

We can use the forces for diamagnetic drag and PR drag (Equations 8 and 6 respectively) to calculate the Alfvén radius of the system, the point at which the force to to magnetism is expected to dominate over PR drag (Hogg, Cutter, and Wynn 2021). This is done by equating the two forces and solving for distance. We assume the maximum possible force from PR drag and so take the unshielded case, and take the weakest case diamagnetic force around the equator:

$$R_p^2 \frac{B_\star^2}{8\pi}\left(\frac{R_\star}{r}\right)^6 = \frac{R_p^2 R_\star^2 \sigma T^4}{r^2 c} \tag{14}$$

Solving this for the distance (r) gives us the Alfvén radius:

$$R_N = \left(\frac{cB_\star^2 R_\star^4}{8\pi\sigma T^4}\right)^{1/4} \tag{15}$$

Where R_N is the radius of magnetic dominance, c is the speed of light $B_\star$ is the magnetic field strength at the surface of the WD, $R_\star$ is the radius of the WD, and T is the temperature of the WD. We see from this that the force due to the magnetic field will dominate at all expected distances at which debris discs are expected to be found.

From Figure 2 we see that at high magnetic field strengths, especially for objects close to the WD, the force from diamagnetic drag dominates that of all forms of PR drag. Despite this we will still be required to simulate PR drag so that systems with weak magnetic fields can still be simulated and in order to bring our model in line with previous models so that our results are comparable.

3.1.5 Co-rotation Radius

The radius of co-rotation refers to the distance at which the velocity of particles in orbit around a star matches the rotation rate of the star's magnetic field. When the orbit is circular and the star in question is a WD, this radius can be determined by the following formula (Hogg, Cutter, and Wynn 2021):

$$R_{co} = \left(\frac{GM_{WD}}{\Omega_{mag}^2}\right)^{1/3} \tag{16}$$

Where G is the universal gravitational constant, M_{WD} is the white dwarf mass, and Ω_{mag} is the magnetic field's angular velocity. This radius will be especially important to our investigation as we intend to vary the angular velocity of our simulated WD.

3.1.6 Tidal Disruption Radius

The radius at which a celestial body would be torn apart by the gravitational forces of a star is known as the tidal disruption radius. This value varies based on the body's density and tensile strength, but typically is approximately one solar radius for an average rocky object orbiting a WD (Hogg, Cutter, and Wynn 2021):

$$R_{TD} = 1R_\odot \tag{17}$$

We expect our simulated asteroids to be broken up within this distance and so expect the periapsis of our accretion discs to be within $1R_\odot$ of the WD.

3.1.7 Mathematical Observations

As diamagnetic drag is caused via motion perpendicular to the magnetic field lines we will be required to adjust the force felt on the particles based on their angle of motion to the field. This will be done by taking the cosine of the angle between relative motion between the field and the particle (v_r), and the direction of the field lines ($B(r)$). This can also be done using the unit vector for the field lines which, for Equation 8, is expressed by (Hogg, Cutter, and Wynn 2021):

$$F = -k(r)m_p\left(v_r - \hat{b}(\hat{b}\cdot v_r\right) \tag{18}$$

We also see from Equation 9 that the force felt is inversely proportional to the distance from the WD to the 6th power ($F \propto r^{-6}$), and so we expect the majority of the force delivered to the particle from the magnetic field will be near the particle's periapsis, affecting the height of its apoapsis.

Additionally, from Equation 8, we see that when the particle travels faster than the local magnetic field lines, the force on the particle will oppose its motion and causing it to lose energy and angular momentum ($v_r > 0, F < 0$).

In WDs which spin against the orbit of a particle we should therefore expect to see faster accretion rates.

The opposite is also true with the particle gaining energy and momentum if the field lines move faster than the particle ($v_r < 0, F > 0$). In WDs spinning with the motion of a particle this could lead to significantly slower accretion rates and in cases where the rotation is high enough, the particles would be accelerated out of system.

By comparing the radii found in Equations 15 (R_N), 16 (R_{co}), and 17 (R_{TD}) we can show how each of these distances can affect the physical outcomes of this simulation (Hogg, Cutter, and Wynn 2021):

- $R_N < R_{TD}$: We expect the magnetic effects to have very little affect on the dynamics of the disc as PR drag dominates in these conditions. For the strengths of magnetic field we will be considering, we do not expect this to be typical.

- $R_N > R_{TD}$: Diamagnetic drag is predicted to dominate the forces dictating the motion of particle within the accretion disc. We expect this to be the default conditions for all particles in our simulation.

- $R_N < R_{co}$: Dust particles moving through the WD's magnetic field lines lose angular momentum, slowly being accreted onto the star. We expect this to be the case for the majority of circumstances we intend to investigate, primarily non-rotating WDs and WDs which rotate against the motion of orbiting discs.

- $R_N > R_{co}$: Field lines move faster than particles in the accretion disc which results in the disc gaining angular momentum from the WD, either being pushed into a higher orbit or ejected from the system entirely. This is expected to be the case in WDs with a high rotation rate where their angle of rotation matches the motion of orbiting particles.

While we expect all of these circumstances to be present in certain conditions in our simulations, it is most likely that we will see conditions where $R_N > R_{TD}$ due to how we intend to investigate specifically the effects of diamagnetic drag and so intend to use high magnetic field strengths. Additionally we expect both the $R_N < R_{co}$ and $R_N > R_{co}$ cases to be present depending on the starting orbital conditions and angular velocity of the WD.

3.2 Parameters

In order to produce a simulation which will produce usable data for real world purposes we are required to investigate the parameters we will have to use for all aspects of the model. For this we find the relevant values for WDs, dust particles, and orbital trajectories, as well as various factors relevant to the development of the actual simulation.

3.2.1 Magnetic Field Strength

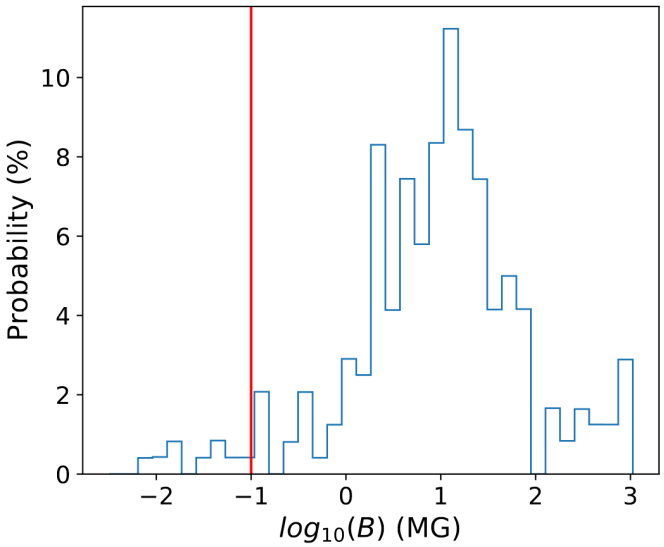

Figure 3: A distribution of observed magnetic WD field strengths (Ferrario, Martino, and Gänsicke 2015). The vertical red line indicates the point where magnetic field strength becomes dominant over PR drag (Hogg, Cutter, and Wynn 2021).

WDs have been observed to show evidence of magnetism with behaviours similar to dipoles. Field strengths vary from as low as 10kG with the highest observed being 800MG (Ferrario, Martino, and Gänsicke 2015). The most common field strength peaks at 1MG with most values falling between 50kG and 10MG for polluted WDs (Kawka and Vennes 2014). 2-20% of all studied WDs show evidence of magnetism (Ferrario, Martino, and Gänsicke 2015; Briggs et al. 2018). For our simulations we will test our model using $1MG$, $100kG$, and $10kG$ field strengths as this will give a wide range of disc lifetimes which will allow us to ensure that the model we produce is accurate over as many cases as possible. It can be seen in Figure 3 that in the majority of cases WD's with magnetic fields have accretion rates dominated by that of diamagnetic drag.

3.2.2 White Dwarf Mass

The distribution of WD masses has a range between $0.2M_\odot$ and $1.4hM_\odot$ also known as the Chandrasekhar limit (Chandrasekhar 1931). The majority of WDs exhibit a mass of about $0.6M_\odot$, whereas magnetic white dwarfs possess an average mass of roughly $0.8M_\odot$. We choose to use a mass of $0.6M_\odot$ as this will allow us to collect results which can be compared with those from Hogg, Cutter, and Wynn (2021).

3.2.3 White Dwarf Radius

Due to how WDs rely on electron degeneracy pressure to prevent gravitational collapse, increasing mass increases the force from gravity but at a higher rate than the resisting force due to electron degeneracy, this additional pressure compresses the star more as its mass increases. We see this by calculating the expected radii from mass using the

mass-radius relation for WDs (Nauenberg 1972):

$$R_{WD} \approx \frac{N^{5/3}\hbar^2}{2m_e G M_{WD}^{1/3}} \tag{19}$$

Where R_{WD} is WD radius, M_{WD} is WD mass, N is the number of electrons per unit mass, m_e is the mass of an electron, $\hbar$ is the reduced Planck constant, and G is the universal gravitational constant. We see from this that as WD mass increases the radius decreases, unlike in other stars. From Equation 19 we calculate an average radius of $0.0126R_\odot$ for a $0.6M_\odot$ WD and a radius of $0.0101R_\odot$ for a $0.8M_\odot$ WD.

3.2.4 White Dwarf Angular Momentum

WDs have a significant range of rotational speeds due to angular velocity maintained from earlier in their lives. Observations show rotational periods ranging from several hundreds of years (Jordan and Friedrich 2002) to 300 seconds (Barstow et al. 1995; Reding et al. 2020). The mean period of a non-magnetic WD is roughly 1 day (Kepler et al. 2017; Kawaler 2003), with magnetic WDs having a average period on the order of years, due to magnetic breaking (Fontaine and Brassard 2008). A range of values for rotational period will be tested between $20000s$ to $500s$, as well as no rotation, as this should allow us to see results both in nominal and extreme cases.

3.2.5 White Dwarf Luminosity

WD temperatures vary over their lifespans, from up to $150,000K$ when first formed, to $6,000K$ after cooling for billions of years, with the majority of observed polluted WD having temperatures less than $25,000K$ (Kawka 2018). Despite magnetic field strength being considered mostly independent of temperature, PR drag is dependent on luminosity, and thus temperature, and so for our simulation we use a typical value of $10,000K$ for temperature.

To calculate luminosity we assume the WD is a black body and use the Stefan-Boltzmann equation:

$$L = \sigma A T^4 \tag{20}$$

Where L is the WD's luminosity, A is the WD's surface area, T is the WD's temperature, and σ is the Stefan-Boltzmann constant. From this we find a typical luminosity of $L \approx 8 \times 10^{27} W$.

3.2.6 Dust Particle Sizes and Densities

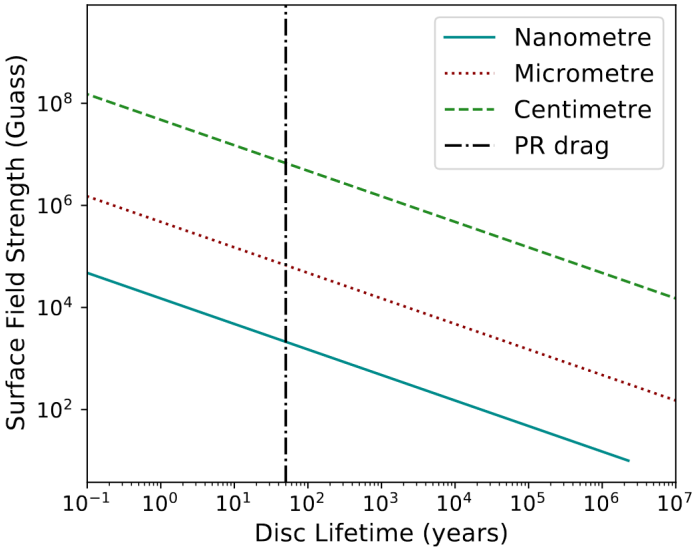

Figure 4: Disc lifetime for various dust particle sizes and magnetic field strengths and PR drag for a 10,000K WD (Hogg, Cutter, and Wynn 2021).

Nanometer sized particles are expected to be removed from the system via radiative forces (Burns, Lamy, and Soter 1979; Burns, Lamy, and Soter 2014) and any particles larger than the micron scale are broken down further by tidal forces. For these reasons most particles present in WD debris discs are thought to be micron sized (Jura 2003; Jura, Farihi, and Zuckerman 2007) with expected life times of 10-100 years (Farihi 2016) as shown in Table 4. Our model will use particles with a radius of one micron $r_p = 1\mu m$ and an average density of $\rho = 2gcm^{-3}$ (Hilton 2002).

3.2.7 Asteroid Masses

Asteroid radii vary greatly with the smallest being around $1m$ and the largest at almost $1000km$ (E. Pitjeva 2004; E. V. Pitjeva and Pitjev 2015). For our asteroid we use a relatively average asteroid with radius $3km$ (Hilton 2002), which at a density of $2gcm^{-3}$ this gives us a total average asteroid mass of $\sim 10^{13}kg$. It should be noted that these are average values for an asteroid in our solar system, though we expect little deviation from this in other parts of the universe.

3.2.8 Asteroid Composition

We justify being able to model our particles as diamagnetic by demonstrating the majority of materials in the atmospheres of polluted WDs have diamagnetic properties. Observations show an abundance of carbon, nitrogen, silicon, and water in the spectral lines of DZ/DAZ WDs (Koester, Gänsicke, and Farihi 2014), all of which are materials with diamagnetic properties. Additionally all observed materials were either ferromagnetic, paramagnetic, or diamagnetic (Hogg, Cutter, and Wynn 2021), and so we are confident that the particles making up our accretion disc will experience a drag force due to their motion through the WDs magnetic field.

3.2.9 Orbital Trajectory

While there are theoretically an infinite number of orbital trajectories a particle could inhabit around a WD, given that most are acquired from asteroid capture and breakup (Jura 2003), in general they will be in highly eccentric orbits with a periapsis a fraction of $R_\odot$. We will use values from Hogg, Cutter, and Wynn (2021) with an semi-major axis $a = 0.4AU$ and an eccentricity $e = 0.9884$, giving an apoapsis at $0.4AU$ and periapsis at $0.5R_\odot$. We are confident that this is an accurate value for the periapsis distance as it is well within the tidal disruption radius calculated in Equation 17. Due to asteroids being most likely to breakup at periapsis, this will be the starting location for all of our simulated particles.

3.2.10 Simulation Cutoff Distances

We simulate particle accretion down to 2 WD radii at which we believe drag forces will be strong enough that particles will accrete to the surface almost instantly. We also do this to avoid inaccuracies in the simulation due to extreme forces close to the WD and to speed up simulation by removing particles which no longer produce meaningful data. Additionally we will simulate particles which are blown out of the system up to $1AU$ away. This ensures the particles reach a distance sufficient for us to say they will never accrete onto the WD and allows for the simulation to be stopped after that point further increasing performance.

3.2.11 Expected Lifetimes

In order to see what the maximum expected particle lifetimes we will be required to simulate are, we use Equation 11 and data from other similar simulations (Hogg, Cutter, and Wynn 2021; Veras et al. 2014). We find that for a WD with a magnetic field of $10kG$ (the lowest force and thus highest simulation time we will be investigating) the maximum particle lifetimes would be around 10^3 years. While this is not a perfect estimate as we will be experiencing more expected force than Equation 11 accounts for, this gives a rough timeline of how long our simulation needs to remain accurate for.

3.3 Model Development

3.3.1 Model Restrictions

An N-Body code will not be required for our simulation as the gravitational influence of the WD is expected to be vastly greater than the influence of any other source. For a number of particles n, implementing N-Body interaction would increase our code's complexity from $O(n)$ to $O(n^2)$, which represents a significant performance loss for relatively no gain in accuracy. We also only simulate the forces on particles and not on the WD itself and set its position to a fixed value at the origin $O(0, 0, 0)$, as these forces would be insignificant and slow the simulation down significantly.

While particles are expected to receive changes to their angular moment from the WD to a noticeable degree we do not expect the reverse to be true due to the ratio of differences between the involved masses. For our average asteroid with a mass of $\sim 10^{13}kg$ we see that the WD has a mass roughly $\sim 10^{16}$ times that of the asteroid which for our purposes has no barring on the results our model will produce.

Particle collisions are expected to occur in these accretion discs as they are a mechanism which determines the size of particles in the disc. However, they are expected to be a secondary condition after the force imparted from the magnetic field as they are expected to dissipate energy but not impact the overall angular momentum of the disc. Due to this we expect collisions should not have a large impact on accretion rates and as simulating these interactions would be very computationally intensive and so we further simplify our code by omitting this from our model.

From our average $\sim 10^{13}kg$ asteroid we find that over $\sim 10^{25}$ of our micron sized dust particles would be delivered into the system at the start of our simulation. It is needless to note that running only one simulation of over one septillion particles for several thousand years would take an inordinate amount of time and due to this we use a significantly reduced number of particles for our models.

For our test simulations we will use an asteroid constructed of 100 particles as this should give us enough variance in starting conditions to fully ensure we get usable results while not increasing code runtime too much. These particles will have randomised positions within a radius of our $3km$ asteroid to roughly simulate how an asteroid would be broken up by WD tidal forces.

As our main investigation is into how different starting conditions affect accretion timescales we will use a single particle for further tests. This will allow us to have more control variables than if a larger more randomised group of particles was used, making our final results more meaningfully reflect how changes to other starting conditions impacted the motion of the particle. Additionally, it has been shown in previous papers on this topic that the average accretion timescales are almost identical for anywhere between 1 and 10,000 simulated particles (Hogg, Cutter, and Wynn 2021).

3.3.2 Runge-Kutta Method

Our simulation uses the 4^{th} order Runge-Kutta method (RK4) to iterate the position of a particle over a given timestep h. This iterative method is required over a simpler method such as Euler's method due to the increased accuracy that will be necessary for dealing with the high forces experienced close to the WD. For a function $f(x)$, RK4 can be expressed by:

$$\frac{dx}{dt} = f(t, x)$$

$$k_1 = f(t_n, x_n)$$

$$k_2 = f(t_n + \frac{h}{2}, x_n + h\frac{k_1}{2})$$

$$k_3 = f(t_n + \frac{h}{2}, x_n + h\frac{k_2}{2})$$

$$k_4 = f(t_n + h, x_n + hk_3)$$

$$x_{n+1} = x_n + \frac{1}{6}(k_1 + 2k_2 + 2k_3 + k_4)h \tag{21}$$

Where k_1, k_2, k_3, and k_4 are slopes of the curve $f(t, x)$ at different points along the interval t_0+h. By averaging these slopes, and giving higher weight to k_2 and k_3 (the slopes

at the midpoint $t_0 + h/2$), we can produce an estimate of the next point along our function to a relatively high degree of accuracy. The use of these midpoints of the curve at half timesteps produces more accurate results by sampling the slope at more points along the function allowing for a better prediction of where the next point should be. This improves on Euler's method which only predicts the position of the next point based on the current slope.

3.3.3 Softening Factors

While RK4 will produce accurate results in most cases, high forces will cause particles to move too far in a single timestep causing inaccuracies in simulations. As this will occur at close distances to the WD, we add a small softening factor to equations of force which include a term for orbital distance. Equation 5 is then altered to:

$$F_g = G\frac{M_{WD}m_p}{(r+\epsilon_G)^2} \tag{22}$$

Equation 6 is altered to:

$$F_{PR} = \frac{v}{c^2}W = \frac{{r_p}^2 L_{WD}}{4c^2}\sqrt{\frac{GM_{WD}}{(r+\epsilon_{PR})^5}} \tag{23}$$

And Equation 9 is altered to:

$$k(r) = k_0\left(\frac{r+\epsilon_D}{R_\star}\right)^{-6}\sqrt{(1+3\frac{z_p^2}{r+{\epsilon_D}^2}} \tag{24}$$

Where ϵ_G, ϵ_{PR}, and ϵ_D are the respective softening factors. This will be especially necessary in Equation 9 as the force is proportional to r^{-6}. Implementing these softening factors ensures that rapid increases of force on particles close to WD do not require lowering the timestep and keeping compute time low. Additionally as this softening is expected to have the largest effect when particles are almost completely accreted it should not affect our results as these particles should already be near the end of their expected lifetimes.

3.3.4 Rotation Matrices

In order to simulate a WD where the magnetic moment is at a different axis than the angular momentum we must us a matrix to rotate the magnetic moment so that at any given time it points in the expected direction as given by the angle and magnitude of the angular momentum. This is done using a generalised form of the 3 matrices used to rotate a point around a sphere by an angle in each dimension:

$$R_x(\theta) = \begin{bmatrix} 1 & 0 & 0 \\ 0 & cos\theta & -sin\theta \\ 0 & sin\theta & cos\theta \end{bmatrix}$$

$$R_y(\theta) = \begin{bmatrix} cos\theta & 0 & sin\theta \\ 0 & 1 & 0 \\ -sin\theta & 0 & cos\theta \end{bmatrix}$$

$$R_z(\theta) = \begin{bmatrix} cos\theta & -sin\theta & 0 \\ sin\theta & cos\theta & 0 \\ 0 & 0 & 1 \end{bmatrix} \tag{25}$$

Where $R_x(\theta)$, $R_y(\theta)$, and $R_z(\theta)$ are the matrices which respectively rotate a vector around the x, y, and z axis by an angle of θ. These will be used in conjunction with each other to rotate the angle of the magnetic moment. Each one of these matrices represents an anticlockwise rotation around their respective axis, for which $R_x(\theta)$, $R_y(\theta)$, and $R_z(\theta)$ will be calculated from the WD's moment of angular velocity.

3.3.5 Code Development

Initial development of the code used for our simulations was done in *Python* due to the language's ease of use, making prototyping and testing changes simple. Use of *Python* also allowed for graphs to be produced easily with *Matplotlib* leading to easy data visualisation. All of our code is designed to work in 4 dimensional space-time as this will be required to produce data for non-equatorial orbits, and in situations where angular momentum and magnetic moment lie on differing axes.

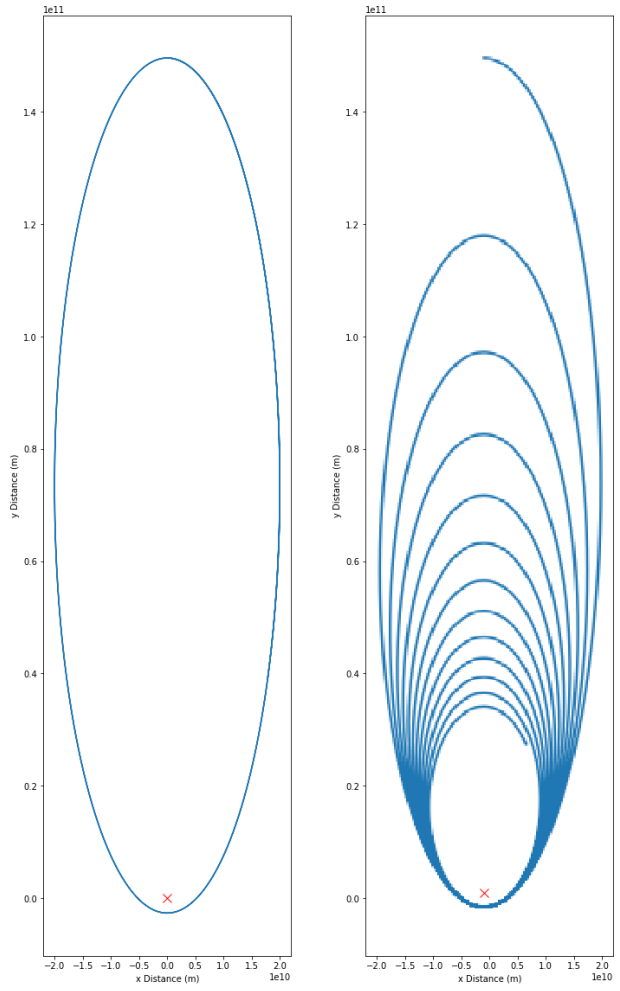

Figure 5: Eccentric orbital simulation results. The left plot displays an orbit with only the force due to gravity, while the right incorporates PR drag and the diamagnetic drag force.

We first implemented the force on due to gravity from Equation 22 on a dust particle in an eccentric orbit around an object with the mass of a WD using $RK4$ as our iterative method. In order to ensure angular velocity would be conserved over large timescales we ran a simulation over the expected maximum length of 1000 years, producing the orbit seen in the left plot in Figure 5. From these initial results we see no deviation in the orbit as expected, and so

are confident in the accuracy of our calculation of gravitational force and our implementation of $RK4$. We further ensured accuracy of our implementation by calculating the particle's angular momentum at each point in the orbit, finding no major discrepancies over the 1000 years.

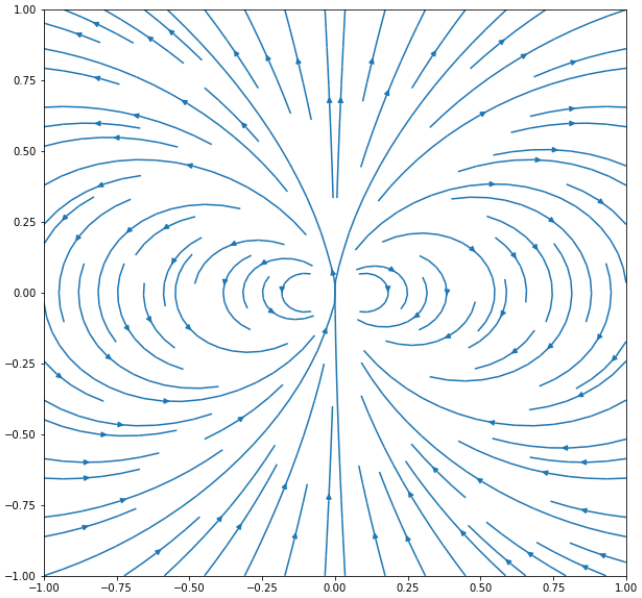

Figure 6: Visualisation of the vector field produced by a dipole.

In order to calculate the force due to the magnetic field we are required to calculate the magnetic field strength and direction around a dipole. This was done using Equation 7 and is visualised with the plot in Figure 6. We then use this field to calculate the force felt on a particle at a given time and position using Equation 8 producing the initial the right plot of 5. This was also the point at which we began to experiment with simulating multiple particles at slightly randomised positions, leading to the thickness visible in the plot on the left of the figure. The data shown is not representative of our final results as many parameters were using stand in values.

Now that we had produced a working simulation of diamagnetic drag, we began to implement the rotation of the WD. Using a vector for angular momentum we produced a function to calculate how the magnetic field would move with the WD's rotational rate at a point at a point in space around the WD. Once this was confirmed to work correctly, the rotation matrices from Equation 25 were implemented to rotate the WD's magnetic moment situations where the magnetic moment was at a different axis to the angular momentum. We also implemented the force due to PR drag at this point, testing to ensure that it worked correctly in systems with no magnetic fields.

At this point simulations of one particle for one year were taking up to several minutes to complete and so in order to run simulations up to the length of our predicted maximum in a reasonable time frame we were required to optimise our code. This was done by rewriting the entire model in $C\#$ due to its significant performance improvements over $Python$ for simulations of this nature. Various other code optimisations were also done during this rewrite which brought the time required to run the previous simulation down to just over 100 milliseconds.

In order to collect and visualise data from this $C\#$ model we then wrote all important values for particle distance at each time to a text file, which could then be loaded back into $Python$ to investigate further and so that the same $Matplotlib$ functions could be used to produce graphs of the data.

3.3.6 Tuning timestep and softening parameters

Now that the code was completed we were required to choose a step size which our implementation of RK4 would use to iterate particle positions. Too large a value of dt would result in simulation results being unusable due to the how this would induce inaccuracies, while too small a value would result in diminishing returns for accuracy while increasing the time taken for each simulation significantly.

After some testing we settled on a value of 10 seconds for the timestep ($dt = 10$), as this appeared to result in acceptable runtimes while not providing noticeable improvements to accuracy over shorter timesteps. We also see from previous papers that a timestep of 10s is acceptable for the magnetic field strengths we plan to use (Hogg, Cutter, and Wynn 2021).

Through testing we found that due to the implementation of RK4, softening parameters were not required in most circumstances, only being required to stop simulational stiffness at very close distances to the WD. Due to this only a fraction of the WD's radius was required as a softening factor as particles were removed from the simulation at 2 WD radii anyway.

4 Results and Discussion

4.1 Simulation Test

Magnetic Field Strength	**Disc Lifetime (Yr)**	
	Test Data	Our Data
1MG	0.0661	0.0658
100kG	8.247	8.075
10kG	248.8	231.6

Table 1: Comparisons of our values for the accretion timescale against data from Hogg, Cutter, and Wynn (2021).

Initially, in order to ensure model accuracy, we ran a set of preliminary simulations based on starting conditions from Hogg, Cutter, and Wynn (2021) with their typical WD values of $M_{WD} = 0.6M_{\odot}$ and $R_{\star} = 0.0126R_{\odot}$ and orbital values of $a = 0.2AU$ and $e = 0.9884$ (apoapsis at $0.4AU$ and periapsis at $0.4R_{\odot}$). We simulated 100 particles starting at the orbital periapsis and simulated them as they accreted down to a distance of 2 WD radii ($r = 2R_{\star}$), finding the disc lifetimes in Table 1. This was done in order to ensure both that our results matched previously collected data, but also to verify previous results so that we could be sure of the accuracy of both models.

While see some differences between our results and the test data this is likely do to how the initial conditions for each particle was slightly randomised which, over large enough timescales, would result in variations in results. Additionally, as the code used to produce the test data is not

publicly available, we are unable to compare our implementations of our iterative methods and so could explain these discrepancies as a difference of methods.

Overall however our results closely mimic the values present in their model over a wide variety of timescales indicating that we are correctly calculating both diamagnetic and PR drag. The fact that we are able to recreate these results to this degree of accuracy gives us confidence in accuracy of our model and indicates that we have a baseline from which we can begin to investigate additional variables.

4.2 Simulation Results

Using the same starting conditions as our test simulations we then investigated the changes imparting angular momentum onto the WD would have on accretion timescales, shown in Table 2. The WD in this data can be though to be spinning anticlockwise about the z axis. The top row of this table (Orbital Plane Angle = 0) represents the WD spinning against the particle's in the accretion disc with the orbital direction of the disc being clockwise about z. The bottom row (Orbital Plane Angle = π) represents the opposite, with the WD spinning with the particle's motion and the accretion disc rotating anticlockwise. Each column in this table contains data from WDs with different rotational periods, with increasing rotational rate moving from left to right.

Accretion and Ejection Timescales (Yr)

Orbital Plane Angle (π)	Period of Rotation (s)						
	∞	20000	10000	5000	2000	1000	500
0	8.075	6.768	5.830	4.569	2.776	1.680	0.938
1/8	7.350	6.168	5.325	4.193	2.576	1.573	0.884
2/8	6.275	5.376	4.720	3.819	2.462	1.560	0.903
3/8	5.651	5.106	4.670	4.024	2.928	2.067	**8.416**
4/8	5.488	5.419	5.315	5.152	**165.573**	**20.579**	**13.801**
5/8	5.651	6.298	6.920	8.392	**73.967**	**9.226**	**2.028**
6/8	6.275	7.575	9.561	19.897	**16.917**	**2.806**	**1.08**
7/8	7.350	9.140	12.226	**941.827**	**7.667**	**2.333**	**1.183**
1	8.075	10.041	13.456	**695.261**	**6.608**	**2.306**	**1.141**

Table 2: Accretion and ejection timescales for a particle at orbiting a $0.6M_{\odot}$ $100kG$ WD, with a semi-major axis of $0.2AU$ and eccentricity of 0.9884. Bold values denote particles which are not accreted but instead are ejected from the system, reaching 1AU from the WD at the listed time.

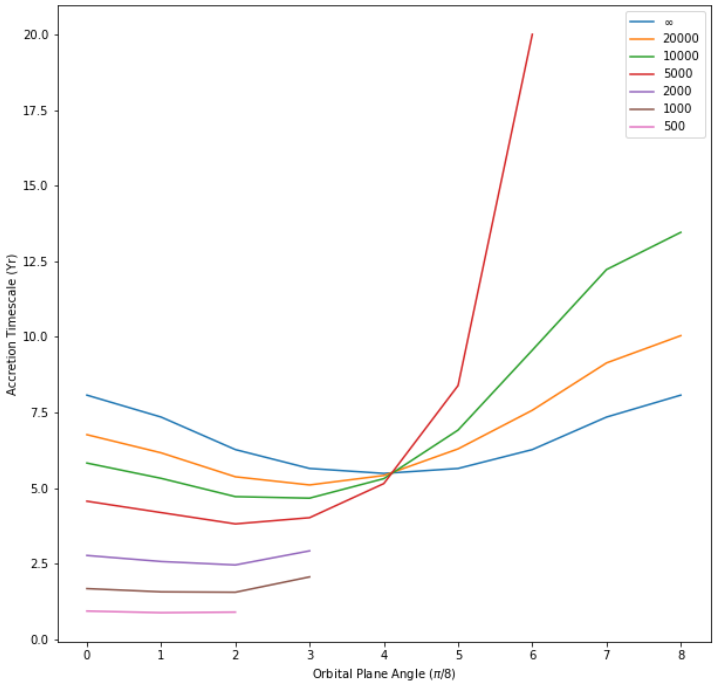

Figure 7: Accretion timescales against orbital plane angle for the data in Table 2. Ejection timescales have been omitted.

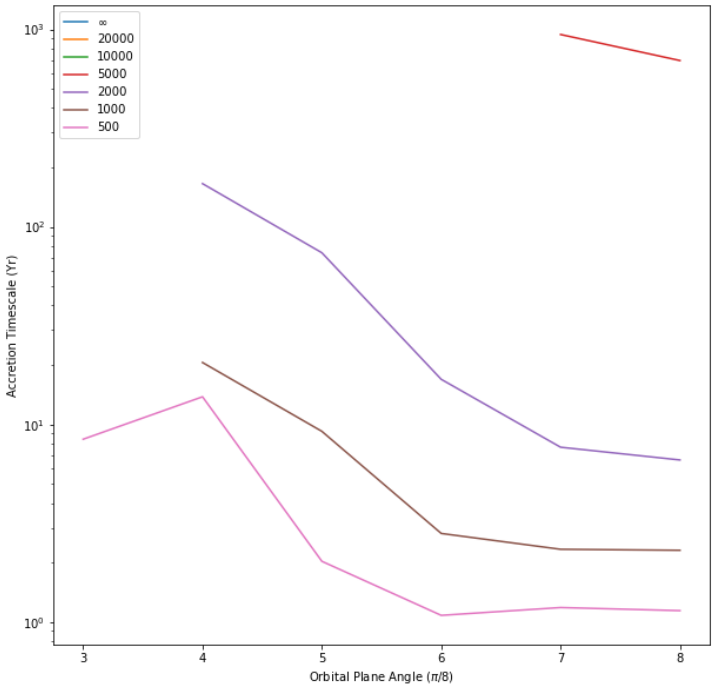

Figure 8: Ejection timescales against orbital plane angle for the data in Table 2. Accretion timescales have been omitted.

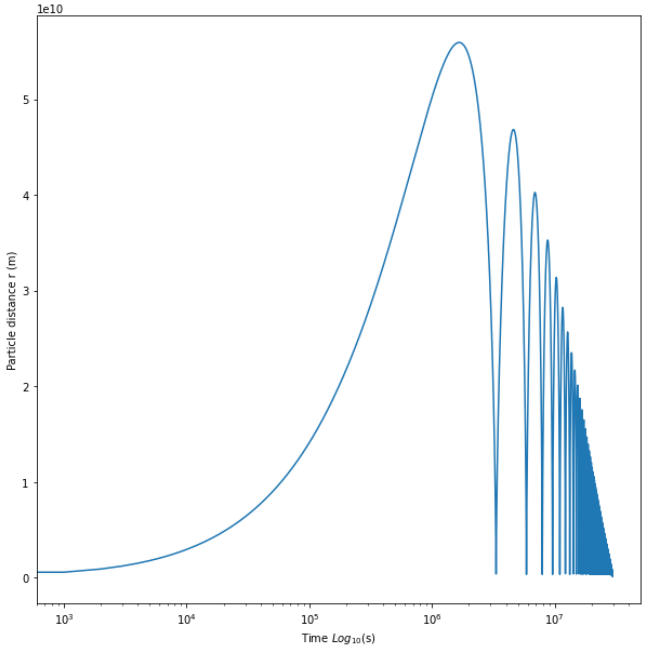

Figure 9: Particle distance from WD against time with an orbital plane angle of 0 and a period of rotation of $500s$ from Table 2.

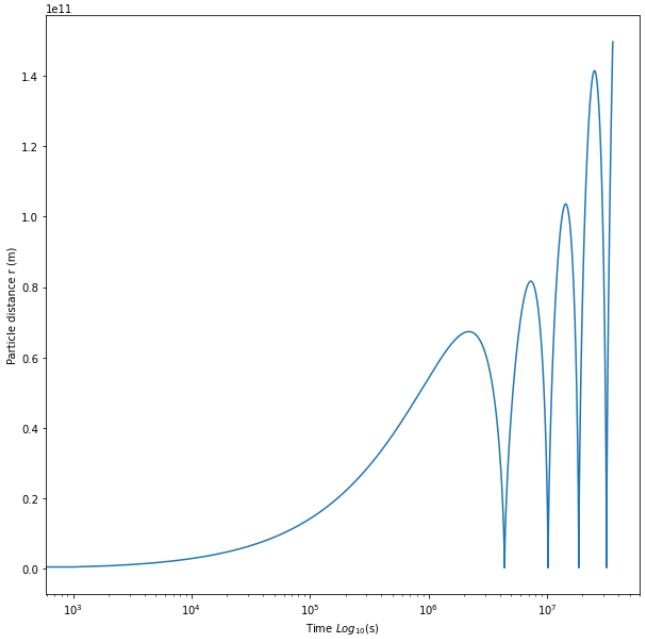

Figure 10: Particle distance from WD against time with an orbital plane angle of π and a period of rotation of $500s$ from Table 2.

We see that the period of rotation can drastically decrease accretion timescales when rotation opposes orbital motion, up to almost an order of magnitude faster in the extreme case of a period of $500s$, visualised in Figure 9. While this is an exceptional condition and we do not expect many WDs to have rotational periods this low, this result does demonstrate the affect that high rotational rates can have on accretion discs.

In the case where the WD spins in the same direction as orbital motion, accretion timescales increase significantly as the period decreases before accretion stops completely and particles are ejected from the system. At these high rotational rates, particles are well within the co-rotation radius calculated from Equation 16 and so are receiving energy from the magnetic field. The ejection timescales here are affected by the period drastically more than accretion timescales with particles reaching $1AU$ over 500 times faster as the rotational period is lowered from $5000s$ to $500s$. Additionally, for these starting conditions, we predict a possible stable orbit at a period between $10000s$ and $5000s$.

These cases where particles are ejected from the system are most clearly seen with Figure 10, where the particle reaches $1AU$ in only 1.141 Years and after only 4 complete orbits. These cases continue to occur up to at least a period of rotation of $5000s$ where particles take almost 700 years to have their periapsis raised to $1AU$. The fact that there is such a large increase in ejection timescale around the period of $5000s$ indicates that this rotational rate may be close to the speed of particles in the disc at their periapsis.

Moving down the rightmost column in Table 2, where the WD does not rotate, we see the impact of how the angle of the orbital plane affects accretion rate. At and angle of 0 and π the orbit is completely equatorial (in a reversed direction at π) and becomes more polar as the angle approaches $\pi/2$ where the apoapsis and periapsis pass over the poles. We see that as the orbit becomes more polar, time scales are reduced, likely due to higher magnetic field strengths present at higher angles from the equator, following the scaling factor $\left(1+3\frac{z_p^2}{r^2}\right)^{1/2}$ in Equation 9.

In cases with both WD rotation and non equatorial orbits we see various interesting results due to the relative motion between the magnetic field and particle not lying on the same plane as the orbit. Between plane angles of $0-\pi/4$, results are almost as expected with faster WD rotation decreasing the accretion timescales but as orbits are not perfectly flat we see some variance in the rate at which a decreasing period of rotation increases the accretion rate.

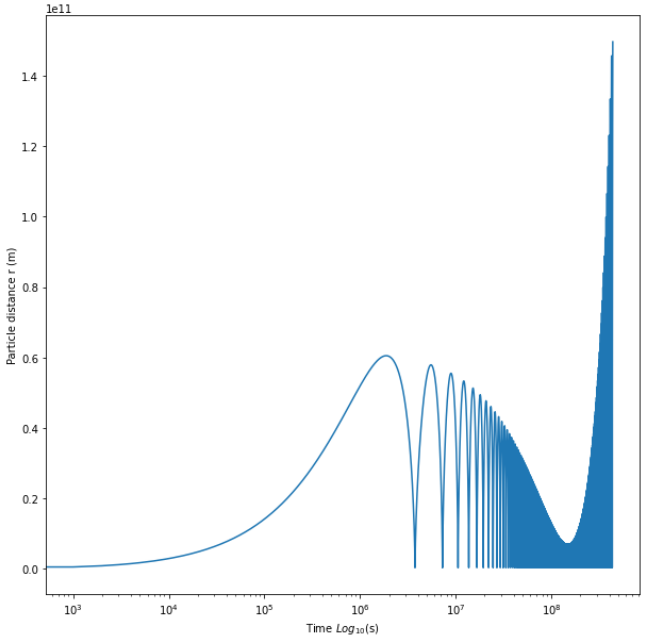

Figure 11: Particle distance from WD against time with an orbital plane angle of $3\pi/8$ and a period of rotation of $500s$ from Table 2.

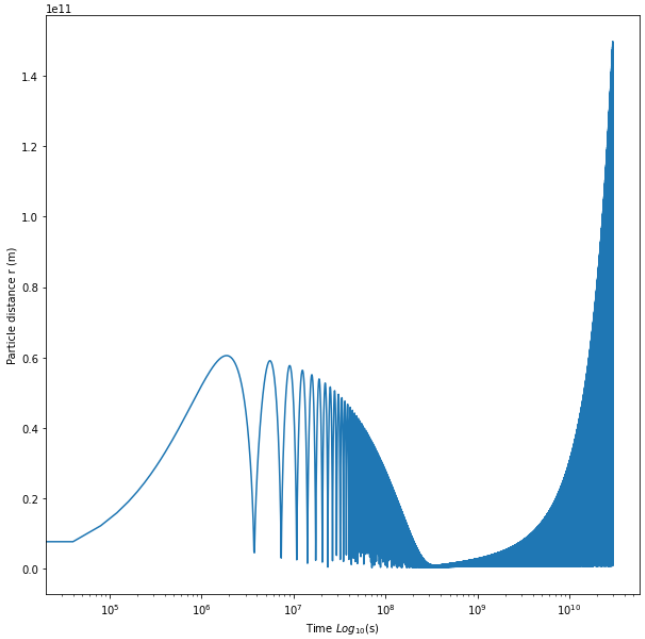

Figure 12: Particle distance from WD against time with an orbital plane angle of $7\pi/8$ and a period of rotation of $5000s$ from Table 2.

As plane angle increases further, we see cases where particles will begin accreting into the WD and then are suddenly ejected, this can be with starting the starting conditions in Figure 11. This occurs due to the force due to diamagnetism shifting the orbital plane of the particle to align to the field. The particle then accelerated quickly by strong magnetic fields close to the star and is ejected from the system. This trend continues with increasing angle becoming a more prominent factor in both increasing accretion time and causing particles to be ejected. It is in this range with a plane angle of $3\pi/4$ and a period of $5000s$ where we observed our highest accretion time of almost 20 years, where our simulated particle was circularised in roughly the same time frame as other particles but took longer to fully accrete as this circularisation had moved the orbital plane of the disc to one which was almost lined up with the magnetic field.

Increasing this plane angle up to π drastically accentuates this effect with WD with periods as low as $5000s$ able to eject orbiting particles after enough time. The most extreme case we observed is shown in Figure 12, where the particles reached as low as a few WD radii after around 5 years before finally being ejected almost 1000 years later. These results indicate that conditions can exist which result in significantly lower accretion rates, and thus higher accretion timescales, implying that a far higher range of disc lifetimes may be possible than previous models imply.

4.3 Model Limitations

One factor our model was missing was the simulation of particle collisions. While this is not likely to have a huge effect on accretion times on average as, while total angular momentum would remain the same in the disc with or without collisions, each particle could obtain vastly different values in a case where collisions are present.

Following from this another potential issue with our results was the use of relatively low total number of particles in each condition, and while this did not impact the time taken for individual particles to accrete, it did give us a fairly low sample size to determine the average accretion timescale of a full accretion disc. And, if particle collisions were a factor, vastly more particles would need to be simulated for that to have a realistic effect.

Additionally the angular momentum transferred to particles in reality would impact the WDs rotational speed, and while this has no measurable effect on the results we produced, it is a fairly simple and computationally cheap improvement to our model. In situations where a significantly more massive object is captured this could lead to the WD gaining or losing angular momentum as the resulting disc is accreted or ejected, which would affect its rotational period. This could lead to the difference between the velocities of the magnetic field and the particles, affecting the drag force felt on particles.

When running our model we simulated particles down to a distance of 2 WD radii to avoid inducing inaccuracies in our simulation from high forces. While this is an acceptable limitation in the majority of circumstances, since there is a possibility that, for some starting conditions, a particle could accrete down closer than 2 WD radii before its orbital plane aligns with the magnetic field and it is ejected from the system. While this will likely have not affected our results by as we did not find any situations where this occurred, it should be accounted for in future models.

We also only simulated particles up to $1AU$ away from

the WD, assuming any particle reaching this distance would be ejected from the system eventually in the future. While this is applicable in the majority of circumstances, there are situations in which a particle would reach an equilibrium with the magnetic field where the average change in angular momentum over time would reach 0, leading to a very eccentric stable orbit. In order to account for this we would be required to check if a particle had reached escape velocity before removing it from the simulation, instead of only checking its distance from the WD. This would likely increase ejection timescales for ejected particles and would cause our current simulation to run indefinitely for particles in equilibrium, requiring additional calculations to detect stable orbits.

All of these improvements would likely greatly reduce the performance of our code by potentially orders of magnitude. In order to counteract this increased complexity an adaptive timestep could be implemented by calculating both RK4 and the higher order RK5 method, decreasing the timestep size if the difference between these two values is too high, this is also known as the Runge–Kutta–Fehlberg method (RKF45). This will result in fewer calculations required at large distances with low forces and so the code would perform far better. Adding an adaptive timestep would also improve accuracy at high forces by lowering the timestep size as required.

5 Conclusions

5.1 Summary

In this investigation we have demonstrated the impact that a magnetic WD's angular momentum has over the accretion timescales of orbiting metallic accretion discs. We have also demonstrated that the angle around a white dwarf that an asteroid is captured, and therefore the angle of the resulting accretion disc, can greatly impact the disc's orbital geometry and in some cases cause the accretion disc to be ejected from the WD's gravitational well.

Despite showing that in some circumstances accretion discs are removed from the WD system faster, we also produced results indicating that in many configurations accretion discs can linger in a system for far longer than shown in previous investigations into diamagnetic drag. While more conditions we tested for showed shorter accretion timescales than not, whether this would reflect an increase or decrease for the average timescale would require further analysis.

Additionally, in order to see results with such a wide range of accretion and ejection timescales we were required to investigate WDs with far higher rotation rates than commonly exist from observations. Given that the mean rotational rate for WDs, as previously discussed, is roughly 1 day, almost all accretion timescales around real WDs would lie in the first two columns of Table 2. From this we can imply that for observed WDs the largest factor which impacts the lifetimes of orbiting accretion discs may in fact be the orbital plane of the disc, rather than the period of rotation, as could be implied by looking at the data from a purely computational viewpoint.

Overall we consider our model and the results gathered from it to be a successful continuation of the work done by Hogg, Cutter, and Wynn (2021) in demonstrating the effect of diamagnetic drag around polluted magnetic WDs. While the majority of our collected data reflects conditions present only in rare circumstances, the data gathered does demonstrate that accretion orbital angle and WD rotation rate do affect accretion timescales. As our model also works to simulate the same results as previous papers but also incorporates more parameters we consider it an improvement over other models of this nature.

5.2 Future Work

Though our model has the ability to simulate particles around a WD with a magnetic moment and angular moment at different axes, we did not perform simulations where this was the case. This is mainly due to the fact that the majority of observed magnetic WDs (and magnetic bodies in general) have a magnetic moment in line with their moment of angular momentum so simulating conditions where, for example, the magnetic moment passed through the WD's equator would produce results that, while possible, have very little basis in reality. Additionally we predict that these conditions would produce results with similar timescales to the conditions we did simulate in this paper and so for the required increase in complexity and runtime, we chose to omit investigating this factor for time time being. Further simulations should also be run with different WD magnetic field strengths and accretion disc orbital distances in order to investigate how our model operates in different conditions.

The first obvious improvement to our model would be to simulate far more particles than we used for any of our tests. This would give us a wider range of values for accretion timescale, allowing us to calculate better averages based on more data. This would likely also be a necessary change if we were to simulate particle collisions as in that situation the total number of collisions would be proportional to the number of particles.

One of the largest forces impacting the accretion of particles into a massive body is heating due to friction with contacting other particles. This causes the particles to raise in temperature and emit radiation, lowering the total energy and angular momentum of the accretion disc (Wagoner 2008). While this mainly only takes place in far larger accretion discs than we study in this paper, it is still a factor that could be investigated in the future.

Additional forces due to magnetism could be added to our simulation to see how they would affect disc accretion rates. One of these being the magnetic tension force which is caused by how magnetic field lines warp around a metallic dust particle. Given by the simple equation (Hogg, Cutter, and Wynn 2021):

$$F_w \approx R_p^2 \frac{B(r)^2}{8\pi} \tag{26}$$

Where F_w is the force imparted on the particle from the field lines, R_p is the particle's radius, and $B(r)$ is the magnetic field at the point r. Other magnetic forces could also be simulated such as those which do not apply to purely diamagnetic dust particles, such as those from eddy currents, although this would require a more concrete breakdown of the exact material composition expected to be in these accretion discs in order to balance out the relative strengths of these forces. Implementing the turbulence due to magnetorotational instability would also improve the accuracy

of this model by more accurately simulating the magnetic interactions between particles in the disc.

While implementing more factors into these simulations would likely significantly improve their accuracy and ability to reflect observations, it is likely these improvements would come at a significant cost to code performance, with some requiring several orders of magnitude more simulated particles. The most computationally demanding of these improvements would be those requiring the interactions between particles to be simulated, making complexity increase with $O(n^2)$, rather than $O(n)$ (where n is the number of particles) as is the case for our model. Due to this the next logical step to improving this simulation would be to implement the least expensive factors with the largest expected affect on accretion rates, likely a more accurate model of the forces from the WD's magnetic field.

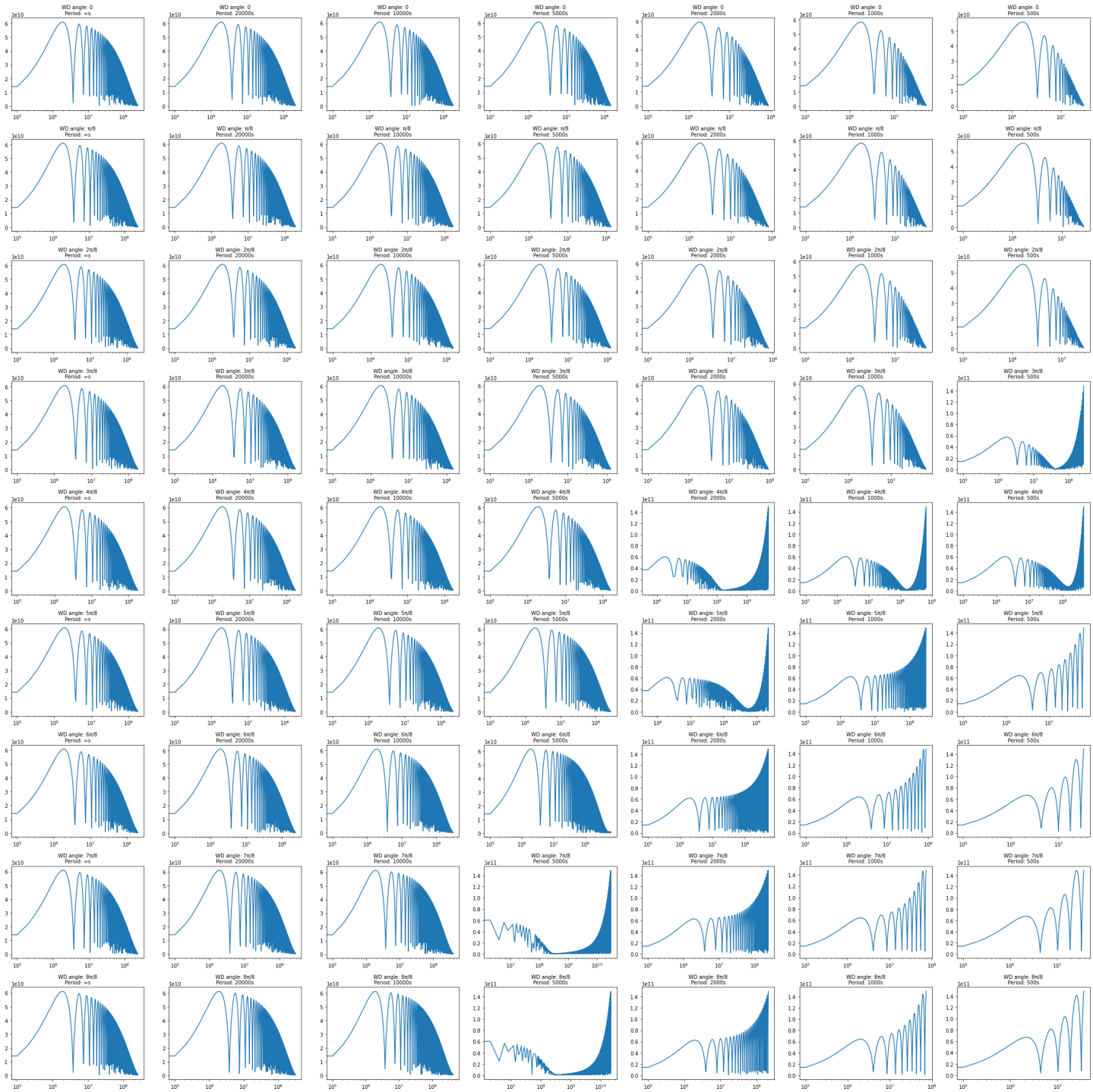

Figure 13: Graphs of particle distance over time for all data points in Table 2.

References

Abd El-Salam, F.A. (2018). "The effects of Poynting–Robertson drag on solar sails". In: *Results in Physics* 9, pp. 897–903. ISSN: 2211-3797. DOI: https://doi.org/10.1016/j.rinp.2018.03.057. URL: https://www.sciencedirect.com/science/article/pii/S221137971732586X.

Balbus, Steven A. and John F. Hawley (July 1991). "A Powerful Local Shear Instability in Weakly Magnetized Disks. I. Linear Analysis". In: *apj* 376, p. 214. DOI: 10.1086/170270.

Bardeen, J., L. N. Cooper, and J. R. Schrieffer (Dec. 1957). "Theory of Superconductivity". In: *Phys. Rev.* 108 (5), pp. 1175–1204. DOI: 10.1103/PhysRev.108.1175. URL: https://link.aps.org/doi/10.1103/PhysRev.108.1175.

Barstow, M. A. et al. (Dec. 1995). "RE J0317-853: the hottest known highly magnetic DA white dwarf". In: *mnras* 277.3, pp. 971–985. DOI: 10.1093/mnras/277.3.971.

Bate, Roger R., Donald D. Mueller, and Jerry E. White (1971). *Fundamentals of Astrodynamics*. New York: Dover Publications.

Berry, M V and A K Geim (July 1997). "Of flying frogs and levitrons". In: *European Journal of Physics* 18.4, p. 307. DOI: 10.1088/0143-0807/18/4/012. URL: https://dx.doi.org/10.1088/0143-0807/18/4/012.

Briggs, Gordon P et al. (May 2018). "Genesis of magnetic fields in isolated white dwarfs". In: *Monthly Notices of the Royal Astronomical Society* 478.1, pp. 899–905. DOI: 10.1093/mnras/sty1150.

Burns, Joseph A., Philippe L. Lamy, and Steven Soter (Oct. 1979). "Radiation forces on small particles in the solar system". In: *icarus* 40.1, pp. 1–48. DOI: 10.1016/0019-1035(79)90050-2.

— (Apr. 2014). "Radiation forces on small particles in the Solar System: A re-consideration". In: *icarus* 232, pp. 263–265. DOI: 10.1016/j.icarus.2013.12.028.

Carroll, Bradley W. and Dale A. Ostlie (2017). *An Introduction to Modern Astrophysics*. 2nd ed. Cambridge University Press. DOI: 10.1017/9781108380980.

Chandrasekhar, S. (July 1931). "The Maximum Mass of Ideal White Dwarfs". In: *apj* 74, p. 81. DOI: 10.1086/143324.

Debes, John H., Steinn Sigurdsson, and Brad Hansen (Aug. 2007). "Cool Customers in the Stellar Graveyard. IV. Spitzer Search for Mid-IR excesses Around Five DAs*". In: *The Astronomical Journal* 134.4, p. 1662. DOI: 10.1086/521394. URL: https://dx.doi.org/10.1086/521394.

Drell, S. D., H. M. Foley, and M. A. Ruderman (Feb. 1965). "Drag and Propulsion of Large Satellites in the Ionosphere; An Alfvén Propulsion Engine in Space". In: *Phys. Rev. Lett.* 14 (6), pp. 171–175. DOI: 10.1103/PhysRevLett.14.171. URL: https://link.aps.org/doi/10.1103/PhysRevLett.14.171.

Farihi, J. (Apr. 2016). "Circumstellar debris and pollution at white dwarf stars". In: *New Astronomy Reviews* 71, pp. 9–34. DOI: 10.1016/j.newar.2016.03.001.

Farihi, J., T. von Hippel, and J. E. Pringle (Aug. 2017). "Magnetospherically-trapped dust and a possible model for the unusual transits at WD 1145+017". In: *Monthly Notices of the Royal Astronomical Society: Letters* 471.1, pp. L145–L149. DOI: 10.1093/mnrasl/slx122.

Farihi, J., M. Jura, and B. Zuckerman (Mar. 2009). "Infrared Signatures of Disrupted Minor Planets at White Dwarfs". In: *The Astrophysical Journal* 694.2, pp. 805–819. DOI: 10.1088/0004-637x/694/2/805.

Ferrario, Lilia, Domitilla de Martino, and Boris T. Gänsicke (May 2015). "Magnetic White Dwarfs". In: *Space Science Reviews* 191.1-4, pp. 111–169. DOI: 10.1007/s11214-015-0152-0.

Fontaine, G. and P. Brassard (Oct. 2008). "The Pulsating White Dwarf Stars". In: *pasp* 120.872, p. 1043. DOI: 10.1086/592788.

Fontaine, G., P. Brassard, and P. Bergeron (Apr. 2001). "The Potential of White Dwarf Cosmochronology". In: *pasp* 113.782, pp. 409–435. DOI: 10.1086/319535.

Griffiths, David J (2013). *Introduction to electrodynamics*. Pearson.

Guess, A. W. (May 1962). "Poynting-Robertson effect for a spherical source of radiation". In: *apj* 135, pp. 855–866. DOI: 10.1086/147329.

Hilton, James L. (2002). "Asteroid Masses and Densities". In.

Hogg, M. A., R. Cutter, and G. A. Wynn (Jan. 2021). "The effect of a magnetic field on the dynamics of debris discs around white dwarfs". In: *mnras* 500.3, pp. 2986–3001. DOI: 10.1093/mnras/staa3316. arXiv: 2009.03444 [astro-ph.SR].

Jordan, S. and S. Friedrich (Feb. 2002). "Search for variations in circular-polarization spectra of the magnetic white dwarf LP 790-29". In: *aap* 383, pp. 519–523. DOI: 10.1051/0004-6361:20011684. arXiv: astro-ph/0201122 [astro-ph].

Jura, M. (Feb. 2003). "A Tidally Disrupted Asteroid around the White Dwarf G29-38". In: *apjl* 584.2, pp. L91–L94. DOI: 10.1086/374036. arXiv: astro-ph/0301411 [astro-ph].

Jura, M., J. Farihi, and B. Zuckerman (July 2007). "Externally Polluted White Dwarfs with Dust Disks". In: *The Astrophysical Journal* 663.2, pp. 1285–1290. DOI: 10.1086/518767.

Kawaler, Steven D. (2003). *White Dwarf Rotation: Observations and Theory*. arXiv: astro-ph/0301539 [astro-ph].

Kawka, Adéla (2018). *The properties and origin of magnetic fields in white dwarfs*. arXiv: 1801.05602 [astro-ph.SR].

Kawka, Adéla and Stéphane Vennes (Jan. 2014). "The polluted atmospheres of cool white dwarfs and the magnetic field connectionding72". In: *Monthly Notices of the Royal Astronomical Society: Letters* 439.1, pp. L90–L94. DOI: 10.1093/mnrasl/slu004.

Kepler, S. O. et al. (Jan. 2017). "White Dwarf Stars". In: *International Journal of Modern Physics Conference Series*. Vol. 45. International Journal of Modern Physics Conference Series, 1760023, p. 1760023. DOI: 10.1142/S2010194517600230. arXiv: 1702.01134 [astro-ph.SR].

King, A. R. (Mar. 1993). "The accretion of diamagnetic blobs by a rotating magnetosphere." In: *mnras* 261, pp. 144–148. DOI: 10.1093/mnras/261.1.144.

Koester, D., Boris T. Gänsicke, and J. Farihi (June 2014). "The frequency of planetary debris around young white dwarfs". In: *aap* 566, A34, A34. DOI: 10.1051/0004-6361/201423691. arXiv: 1404.2617 [astro-ph.SR].

Kuestler, Gerald (July 2007). "Diamagnetic levitation - Historical milestones". In: *Revue Roumaine des Sciences Techniques - Serie Électrotechnique et Énergétique* 52, pp. 265–282.

Nauenberg, Michael (June 1972). "Analytic Approximations to the Mass-Radius Relation and Energy of Zero-Temperature Stars". In: *The Astrophysical Journal* 175, p. 417. DOI: 10.1086/151568.

Newton, Isaac (1726). *Philosophiæ naturalis principia mathematica*. Editio tertia, aucta & emendata. Londini : Apud G. & J. Innys, 1726.

Pitjeva, E. (Jan. 2004). "Estimations of masses of the largest asteroids and the main asteroid belt from ranging to planets, Mars orbiters and landers". In: 35, p. 2014.

Pitjeva, E. V. and N. P. Pitjev (2015). "Masses of asteroids and total mass of the main asteroid belt". In: *Proceedings of the International Astronomical Union* 10.S318, pp. 212–217. DOI: 10.1017/S1743921315008388.

Rafikov, Roman R. (Apr. 2011). "Metal accretion onto white dwarfs caused by Poynting-Robertson drag on their debris disks". In: *The Astrophysical Journal* 732.1, p. L3. DOI: 10.1088/2041-8205/732/1/l3.

Reding, Joshua S. et al. (May 2020). "An Isolated White Dwarf with 317 s Rotation and Magnetic Emission". In: *apj* 894.1, 19, p. 19. DOI: 10.3847/1538-4357/ab8239. arXiv: 2003.10450 [astro-ph.SR].

Robbin, Joel W. (Jan. 1981). "Foundations of Mechanics (Ralph Abraham and Jerrold E. Marsden)". In: *SIAM Rev.* 23.1, pp. 120–121. ISSN: 0036-1445. DOI: 10.1137/1023027. URL: https://doi.org/10.1137/1023027.

Veras, Dimitri et al. (Oct. 2014). "Formation of planetary debris discs around white dwarfs textendash I. Tidal disruption of an extremely eccentric asteroid". In: *Monthly Notices of the Royal Astronomical Society* 445.3, pp. 2244–2255. DOI: 10.1093/mnras/stu1871.

Wagoner, Robert V. (2008). "Relativistic and Newtonian diskoseismology". In: *New Astronomy Reviews* 51.10. Jean-Pierre Lasota, X-ray Binaries, Accretion Disks and Compact Stars, pp. 828–834. ISSN: 1387-6473. DOI: https://doi.org/10.1016/j.newar.2008.03.012. URL: https://www.sciencedirect.com/science/article/pii/S1387647308000146.

Wynn, G. A. and A. R. King (July 1995). "Diamagnetic accretion in intermediate polars – I. Blob orbits and spin evolution". In: *Monthly Notices of the Royal Astronomical Society* 275.1, pp. 9–21. ISSN: 0035-8711. DOI: 10.1093/mnras/275.1.9. eprint: https://academic.oup.com/mnras/article-pdf/275/1/9/18539668/mnras275-0009.pdf. URL: https://doi.org/10.1093/mnras/275.1.9.

Xu, S. and M. Jura (Jan. 2012). "Spitzer Observations of White Dwarfs: The Missing Planetary Debris around DZ Stars". In: *apj* 745.1, 88, p. 88. DOI: 10.1088/0004-637X/745/1/88. arXiv: 1109.4207 [astro-ph.EP].

Zuckerman, B. et al. (Oct. 2003). "Metal Lines in DA White Dwarfs". In: *apj* 596.1, pp. 477–495. DOI: 10.1086/377492.

Lay Summary

White dwarfs are the final stage of evolution for stars with masses similar to that of our Sun or slightly higher. When these stars run out of fuel, they go through a series of transformations, eventually collapsing into a dense core known as a white dwarf. Despite their small size, white dwarfs are incredibly dense, with masses comparable to that of the Sun packed into a space roughly the size of the Earth. Due to this density, white dwarfs are some of the most luminous objects in the sky, emitting intense radiation across the electromagnetic spectrum. Magnetic white dwarfs are a subclass of white dwarfs that possess strong magnetic fields, typically ranging from tens of thousands to hundreds of millions of times stronger than the Earth's magnetic field.

Accretion discs are rotating disks of gas and dust that surround celestial objects such as stars, black holes, and neutron stars. These disks are formed when material from a companion star or a cloud of gas and dust is gravitationally attracted to the central object, forming a flat disc-like structure. Magnetic white dwarfs can accrete material from various sources, but it is often thought to be derived from the disruption of asteroids that are gravitationally captured by the magnetic white dwarf. These captured asteroids are then broken apart into small dust particles by tidal forces created from strong gravity close to the white dwarf, forming an accretion disc. The dynamics of these accretion discs are complex with their motion mainly depending on the white dwarf's mass, magnetic field strength, and spin.

Previous simulations, which investigated only the affects of the mass and field strength of a white dwarf on an accretion disc, produced values for the accretion timescale of discs (the time taken for the disc to fully accrete onto the white dwarf) which do not fully align with real world observations. In reality we see that far fewer magnetic white dwarfs harbour accretion discs than current simulations would suggest, implying that their accretion timescales are lower than what simulations predict. This is known as the missing disc problem.

In spinning white dwarfs we expect the magnetic field to also rotate causing the relative speed between a disc and the field lines to either increase or decrease depending on the direction of the spin. This results in a respective increase or decrease in drag on dust particles in the disc from the magnetic field which could drastically affect accretion timescales. Additionally, there may be cases in which a white dwarf could rotate fast enough that, instead of causing drag, the magnetic field would impart energy onto an orbiting disc, causing it to be ejected from the white dwarf's gravitational influence.

In this research paper, we focus specifically on the dynamics of magnetic white dwarf accretion discs, using numerical simulations to model the motion of particles in these discs in cases where the white dwarf has angular momentum, also investigating situations where accretion discs are at various angles to this axis of rotation. The goal of these simulations was to produce a more accurate model of white dwarf accretion dynamics in the hope that it would produce results which could help explain the missing disc problem.

We began by producing a simulation of gravity using Newton's laws, this allowed us to model the motion of particles in an accretion disc around a point in space. In order to simulate the drag on these particles, we simplified the white dwarf's magnetic field into a dipole (essentially a large bar magnet), and by spinning this field with a given period of rotation, we were able to produce the conditions around a magnetic white dwarf after the tuning of some parameters. Within this system we were able to choose the starting position and velocity of dust particles which would most closely represent those found in an average accretion disc. We then ran this simulation with various white dwarf spin rates and particle starting conditions, in some cases for up to 1000 years, until we were satisfied that we could draw conclusions from the data.

Through our simulations, we found that the spin of a white dwarf can significantly affect the accretion timescale of its disc, decreasing it by up to an order of magnitude in extreme conditions. We also found that accretion discs which passed over the poles of a white dwarf, instead of the equator, experienced far more magnetic drag and so were accreted faster than those in a more traditional orbit. Additionally, we saw that in certain configurations of spin and orbital plane particles can be accelerated from the magnetic field and ejected from the white dwarf's gravitational well.

This investigation produced results which indicate accretion timescales are lower on average than other simulations of a similar nature, shedding additional light onto the processes affecting accretion discs around magnetic white dwarfs, helping to explain the missing disc problem by explaining some real world observations. These results have important implications for our understanding of the evolution of magnetic white dwarfs and their surrounding accretion discs. In particular, by finding that the spin of the white dwarf plays a significant role in determining the accretion timescale of its disc and showing the new phenomena wherein particles will be ejected from the white dwarf's gravitational well under certain conditions.

These findings have important implications for future studies of not only magnetic white dwarfs, but large scale magnetic systems in general by showing that the rotation of a magnetic field can have a massive impact on dynamics within a system.